Renewable Energies Offshore – Guedes Soares (Ed.)
© 2015 Taylor & Francis Group, London, ISBN: 978-1-138-02871-5

The influence of support structure dynamics on floating wind turbine performance

K. Cuschieri & T. Sant
Department of Mechanical Engineering, University of Malta, Msida, Malta

R.N. Farrugia
Institute for Sustainable Energy, University of Malta, Msida, Malta

ABSTRACT: A full-scale offshore wind turbine was simulated with two different floating platform concepts, a Tension Leg Platform (TLP) and a floating spar, to examine the impact of platform motion on the rotor power performance. The study was restricted to regular wave conditions and constant wind speeds below the rated value. Combinations of the surge, pitch, and heave degrees of freedom were considered and simulated in *FAST* to determine the time-varying platform displacements. The latter were then prescribed to *WInDS*, a lifting-line free-wake vortex model. The means and peaks of the time series predictions for the rotor power coefficient under floating conditions were calculated both with *FAST* and *WInDS*. The results were compared to those under non-floating conditions. While the influence of the platform motion on the time-averaged rotor power output was found to be very small, the corresponding peak-to-peak values under certain conditions were found to be considerable.

1 INTRODUCTION

1.1 *Background research and motivation*

Since its inception in the 1920s (Hewson 1975) wind turbine technology has evolved substantially such that it is regarded as one of the most advanced and commercially mature technologies available today that can effectively mitigate challenges related to climate change and energy security. The last decade has seen the development of the offshore wind sector, with the marinisation of the established onshore wind turbine technology in order to be capable of withstanding the offshore environment (EWEA 2013). However, present offshore technology is restricted to shallow water areas with bottom-mounted fixed support structures. Today, there is increased interest to develop floating solutions, adapted from the oil and gas industry, to be able to support offshore wind turbines in deep waters where vast wind resources exist in areas where environmental and planning issues are less prohibitive (Butterfield et al. 2005). Therefore, current research is being focused on the development of cost-effective floating wind turbine solutions which, unlike bottom-mounted concepts, are not restricted to particular sea depths. Such deep offshore technology has not yet been made commercially available, though multiple nations are working towards systems having a cost of energy that is competitive with other popular power generation technologies. In fact, full-scale prototypes have already been installed to test the technology. These include the Windfloat, Hywind, and Fukushima systems deployed in Portugal, Norway, and Japan, respectively (EWEA 2013).

Deep offshore technology presents a number of engineering challenges due to the complexity of the marine environment to which the wind turbine would be exposed. Substituting the rigid support structure for a floating platform induces multiple degrees of freedom (DOFs) for turbine motion which directly affect the structural integrity and stability of the system. Besides providing buoyancy, the platform must also limit the motion of the system. Consequently, the turbine will be concurrently exposed to aerodynamic, hydrodynamic, gravitational, and inertial loads, with the induced motions on the rotor affecting to a certain extent the power performance characteristics, and hence the energy yield, of the system. The complexity of the aerodynamics of floating turbines implies that certain aerodynamic and energy yield analysis tools normally applied to rigidly-supported systems cannot be directly applied to floating systems. Uncertainty computations in energy yield assessments for the turbine will have to account for the uncertainty resulting from the platform-induced motions. Due to the cubic relationship between the effective wind speed and power, the platform motion may result in an appreciable influence in the energy yield (Butterfield et al. 2005).

To date, most research has concentrated on the structural dynamics aspects of offshore floating technology but an in-depth investigation of the influence on rotor power performance has not been conducted in sufficient detail yet (Henderson et al. 2003, Withee

2004, Jonkman 2007). This paper investigates the impact of platform motion on the power performance characteristics of floating wind turbines. Two different floating platform concepts, the tension leg platform (TLP) and the floating spar were considered. In the absence of experimental data, a numerical approach including the use of a high fidelity free-wake vortex model was adopted to estimate the deviations in the output power from floating rotors as compared to those installed on fixed foundations.

1.2 *Overview and organization of work*

The numerical investigations were performed on the NREL 5 MW baseline offshore wind turbine (Jonkman et al. 2009) installed on the MIT/NREL tension-leg platform (TLP) and OC3-Hywind spar. These were modelled using two tools:

- *FAST*, an aero-hydro-servo-elastic simulator developed by NREL (Jonkman 2007) with the aerodynamics modelled using the blade element/ momentum (BEM) or the Generalised Dynamic Wake-based (GDW) methods, and
- *WInDS*, an open-source lifting-line free wake vortex model developed by the University of Massachusetts Amherst (Sebastian 2012).

In each modelling tool, the systems were subjected to a series of platform motions at three wind speeds below the turbine's rated speed and the corresponding fluctuations in rotor performance were investigated. In both tools the turbine blades and tower were modelled as rigid structural elements. By keeping the modelling settings identical in both tools the differences in recorded results were attributed to the different assumptions and algorithms involved in the BEM/GDW and free-wake vortex methods (FVM). The first step was to derive the rotor performance characteristics for non-floating conditions using both tools and determine the optimal tip speed ratio for each wind speed considered. These are based on the static aerofoil data available for the rotor blades, which had been corrected for 3D effects by Jonkman (2007). The optimal *WInDS* settings were also defined following a numerical convergence analysis.

Once all simulation settings were finalised the wind turbine systems were modelled in *FAST* to derive the platform motions for each motion case and corresponding performance fluctuations. The derived platform motions were then fitted to Fourier functions and prescribed to *WInDS* to obtain the corresponding performance fluctuations. The means, peaks, and amplitudes of the predicted times-series variations in rotor power were analysed for each tool independently and then finally compared.

2 SOFTWARE MODELLING TOOLS

2.1 *FAST (v7.02)*

The Fatigue, Aerodynamics, Structure, and Turbulence (*FAST*) code was developed by NREL and is capable of simulating horizontal axis wind turbines having two or three blades in various conditions, enabling the determination of extreme and fatigue loads. It consists of a number of subroutines coupled together, including the AeroDyn and HydroDyn codes for aerodynamic and hydrodynamic calculations, respectively. These give the code its aero-hydro-servo-elastic capability through which onshore, near-offshore, and deep-offshore floating wind turbines (OFWTs) may be modelled (Jonkman et al. 2005).

Through the use of appropriate switches in the input files, the activation of the 24 DOFs defined in *FAST* may be controlled. These range from platform motion (in the case of OFWTs) to blade flexibility. A number of coordinate systems are also defined to enable kinematic and dynamic calculations of each modelled body (Jonkman 2007).

The purpose of the AeroDyn subroutine is to determine the blade element loads and rotor-wake effects at each blade radial location and time step. It involves two aerodynamic models for the user to choose from: the GDW model and the quasi-steady BEM model. The former is more appropriate for conditions involving dynamic inflow phenomena resulting in rapid changes in angle of attack and flow velocities at the rotor blades. However, it may give erroneous results for wind speeds below 8 m/s as the wake approaches a turbulent state if the induced velocities at the rotor would not be small relative to the free-stream, an assumption upon which it was developed. Below this speed the BEM model is automatically activated, thus ignoring the Prandtl hub and tip loss models that would otherwise have been enabled if the BEM model were activated directly by the user. The code also includes the Beddoes-Leishman model for dynamic stall (Moriarty et al. 2005).

2.2 *WInDS*

The Wake Induced Dynamics Simulator (*WInDS*) was developed at the University of Massachusetts Amherst. This free-wake code is capable of modelling the unsteady evolution of the 3D helical wake emerging from the rotating wind turbine blades in the time domain. This makes it much more physically comprehensive than other codes, such as BEM and GDW, but not as computationally expensive as fully-discretised Navier Stokes solutions. Calculations are based on the Biot-Savart law, which enables the computation of induced velocity at any point due to a vortex filament in the rotor wake (Sebastian 2012). The positions and velocities calculations for each time step are performed using a forward Euler integration scheme and an implicit integrator, forming the predictor-corrector method.

In order to reduce computational times, *WInDS* was modified at the University of Malta to incorporate a wake age cut-off parameter. This signals the number of rotor revolutions after which the near-wake vortex filament induced velocities have negligible influence due to their downstream distance away from the rotor.

Therefore, upon reaching the cut-off point, the grid size would be set and the corresponding vortex filaments beyond a given distance from the rotor-plane are discarded (Farrugia et al. 2014, Sant 2007).

The Ramasamy-Leishman (RL) vortex core model has been implemented in *WInDS* to account for the influence of the viscous effects on the rotor near-wake development. A core growth model for the vortex state transition is defined through the use of the vortex Reynolds number, Re_v, which is the ratio of the vortex circulation strength and kinematic viscosity, ν. The core growth model is expressed as follows:

$$r_c = \sqrt{r_0^2 + 4\alpha_L \nu(1 + a_1 Re_v)t} \quad (1)$$

where r_c = vortex core radius; r_0 = initial core radius; α_L = empirical constant equal to 1.25643; a_1 = empirical constant equal to 6.5×10^{-5}; and t = wake age. The value for r_0 is found through:

$$r_0 = \sqrt{4\delta_\nu \alpha_L \nu t_0} \quad (2)$$

where δ_ν = turbulent viscosity coefficient; and t_0 = initial time.

3 METHODOLOGY

3.1 *Overview*

All *WInDS* simulations were performed on the supercomputing cluster at the University of Malta. This consists of 64 processing nodes, with 12 cores on each node and 32GB memory for each node. The following is an outline of the methodology applied for the study.

1. Derivation and comparison of rotor performance curves under fixed conditions using *FAST* and *WInDS* to identify the optimal tip speed ratio (TSR) for the selected wind speeds;
2. Determination of wave heights and periods for modelled sea conditions;
3. Simulation of both OFWTs in *FAST* and analysis of platform motions;
4. Validation of platform motions against other published works;
5. Numerical study in *WInDS* to identify appropriate parameters for minimising numerical errors;
6. Prescription of *FAST*-derived platform motions of OFWTs from Step 3 in *WInDS* to derive corresponding performance variations;
7. Comparison of floating rotor performance predictions from *FAST* and *WInDS*.

3.2 *Wind turbine rotor*

The NREL 5 MW baseline offshore wind turbine was used throughout the study (Jonkman et al. 2009). It is a three-bladed upwind turbine having a rotor diameter of 126 m, a hub height of 90 m, and cut-in, rated, and cut-out wind speeds of 3 m/s, 11.4 m/s, and 25 m/s, respectively. Each blade is comprised of eight different aerofoil profiles, including two cylindrical profiles at the root. Jonkman (2007) adjusted the aerofoil data to cater for 3D effects and rotational stall delay, the latter of which involved the use of the Selig and Eggars, and Viterna methods for angles of attack between 0° and 90°. The corrected aerofoil data used in this study is available from Jonkman et al. (2009).

Table 1. Wave parameters for regular sea state based on data from BMT ARGOSS (2014).

Wind Speed m/s	Wave Height m	Wave Period s
6	0.5	4.5
7.5	0.7	4.5
10	1.1	4.5

3.3 *Floating platforms modelled*

The design of the MIT/NREL TLP was finalised by Matha (2009) as having 8 mooring lines in tension attached to 4 spokes of length 27 m, set 90° apart. The OC3-Hywind platform is a spar buoy based on the original Hywind concept development by Statoil and was modified to support the NREL 5 MW turbine (Jonkman 2010). The platform has 3 mooring lines in a delta connection configuration set 120° apart.

3.4 *Wind and wave conditions*

Metocean conditions for the Maltese Islands, which are located in the Central Mediterranean sea, were considered in the present study. The long-term average wind speed at a height of 90 m above mean sea level was estimated by Aquilina et al. (2014) to be equal to 7.3 m/s. Therefore, it may be assumed that the turbine will be operating below the rated wind speed of 11.4 m/s for a certain amount of time. Under such conditions maximum operating efficiency is sought given that the generator is only partially loaded. The two OFWT configurations were modelled in these conditions with three different wind speeds: 6 m/s, 7.5 m/s, and 10 m/s. The comparison between *FAST* and *WInDS* was restricted to simple flow conditions under which the wind speed was constant and uniform across the rotor disc. Furthermore, only one-dimensional regular and deep water waves were considered. The presence of wind-wave misalignment was ignored. Wave conditions corresponding to the three wind speeds were derived from wave climate data obtained from BMT ARGOSS (2014). The mean wave height, H_m, and mean period, T_m, for each wind speed are given in Table 1.

3.5 *Modelled operational cases*

The floating platform systems were exposed to different combinations of single- and multi-DOF motions. The purpose was to identify the influence of the motions both individually and when coupled. The 6

Table 2. Cases of platform motion combinations considered.

Case Number	Platform Motion	Degrees of Freedom
1	Surge	1
2	Pitch	1
3	Heave	1
4	Surge + Pitch	2
5	Surge + Heave	2
6	Surge + Pitch + Heave	3

motion cases are outlined in Table 2. These were simulated in *FAST* and *WInDS* for each platform and for each wind speed (6 m/s, 7.5 m/s, and 10 m/s). In all cases the optimal blade pitch of 0° was assumed.

Time series platform motion data predicted by *FAST* for each of the above cases were fitted to a Fourier curve having one sinusoidal function in Matlab. This is given by Equation 3.

$$X = X_0 + A\sin(2\pi ft + \varphi) \tag{3}$$

where A = amplitude; f = frequency; X_0 = initial displacement; and φ = phase difference of motion. The curve-fitting procedure was applied independently to each of the considered DOFs. In all computations, the rotor speed was varied such that the optimal TSR of 7.625 was kept constant.

3.6 *Modelling tool settings for floating turbine analysis*

3.6.1 *FAST*

In all *FAST* computations, a dynamic inflow model was activated. This implied that all aerodynamic computations for wind speeds higher than 8 m/s were conducted with the GDW, whilst for lower wind speeds the BEM model was used. No dynamic stall model was activated in order for the results to be comparable to those from *WInDS*, as the latter does not have any such model incorporated in the code. All DOFs associated with blade and tower flexibility were also deactivated, since *WInDS* can only model rigid blades and towers. The generator DOF was deactivated in order to keep the rotor speed constant.

3.6.2 *WInDS*

The key parameters identified for the *WInDS* computations are outlined in Table 3. Though Farrugia et al. (2014) had already outlined the optimal settings, the effect of number of surge cycles and the number of rotor revolutions under stationary platform conditions on the model were investigated further to confirm numerical convergence. The purpose of the latter was to allow the numerical convergence to be reached prior to the initiation of platform motion. The final list of settings is listed in Table 3.

Table 3. Summary of common settings for *WInDS* simulations.

Parameter	Value
Vortex core growth model	Ramasamy-Leishman
Average turbulent viscosity coefficient	100
Viscosity vortex model number	1 (Scully vortex model)
Number of blade nodes	37
Rotor azimuth angle discretisation	10°
Wake age cut-off parameter	5
Stationary platform rotor revolutions	10
Number of platform motion cycles	5

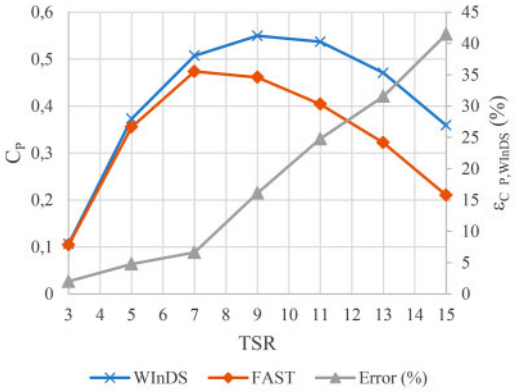

Figure 1. Comparison of power coefficient curves from *FAST* and *WInDS*.

3.7 *Wind turbine rotor performance for fixed non-floating conditions*

Initially the computations with *FAST* and *WInDS* were conducted for a non-floating turbine with a rigid foundation. In *FAST* the BEM inflow model was activated along with the Prandtl tip and hub loss models. The *WInDS* simulations were also run for a fixed number of rotor revolutions whilst the simulation time was decreased with increasing TSR in order to maintain the desired data collection per 10° azimuth angle change of rotor blade position. In fact the downstream distance travelled by the starting wake away from the rotor decreased from approximately 5D at a TSR of 3 to approximately 0.8D at a TSR of 15.

The variations of the rotor power coefficient with TSR predicted by the two codes were compared. The comparison is shown in Figure 1, where the percentage difference between the results, $\varepsilon_{C\_P,WInDS}$, is expressed by the equation:

$$\varepsilon_{C\_P,WInDS} = \left\{1 - \left(C_{P,FAST}/C_{P,WInDS}\right)\right\} \times 100 \tag{4}$$

where $C_{P,FAST}$ = power coefficient result obtained from *FAST*; and $C_{P,WInDS}$ = power coefficient result

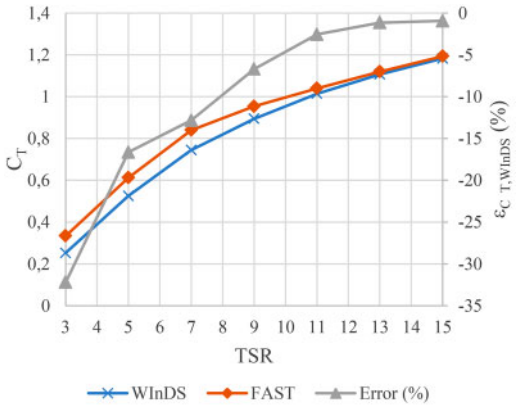

Figure 2. Comparison of thrust coefficient curves from *FAST* and *WInDS*.

from *WInDS*. Figure 2 shows a similar diagram for the rotor thrust coefficient, where the percentage difference between the *FAST* and *WInDS* results, $\varepsilon_{C\_T,WInDS}$, is again expressed similarly to Equation 4.

From the *FAST* results, the TSR corresponding to the maximum power coefficient was identified to be equal to 7.625 for all the three wind speeds. As can be seen from Figure 1, the *WInDS* results for the power coefficient were seen to be larger, with the percentage difference increasing with TSR. As was noted by Sebastian (2012), these differences at large TSRs are primarily attributed to the influence of the starting wake through the wake-induced velocity at the rotor. As the rotor speed increased with TSR the downstream distance travelled by the starting vortex in the time simulated decreased since the number of revolutions was the same for each simulation. Therefore, as the TSR increased the influence of the vortex also increased. As a result, the accuracy of the performance values for high TSRs is questionable due to the minimum distance requirement of approximately 2D. However, the latter requirement is met at the optimal TSR of 7.625. At this TSR value, the discrepancies in the power coefficient between *FAST* and *WInDS* was seen be less than 10% (see Fig. 1). Such discrepancies are more related to the differences in the inherent physical assumptions of the numerical models embedded in the codes.

3.8 *Wind turbine rotor performance for floating conditions*

The influence of platform motion on rotor performance was characterised by deriving time series variations of the power coefficient. The average and peak values from these variations were then determined. Here, the 'peak value' refers to the greatest value of performance coefficient experienced. The average values were then compared to the corresponding performance coefficients of the equivalent fixed

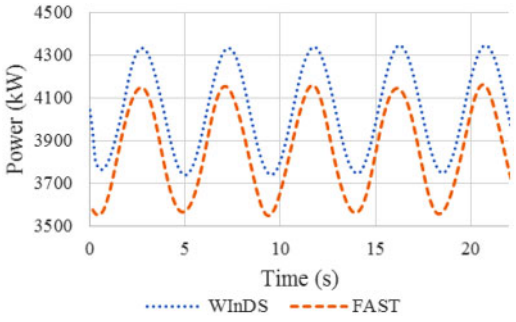

Figure 3. Time series of output power of rotor mounted on the TLP for Case 6 with U = 10 m/s, H_m = 1.1 m, T_m = 4.5 s.

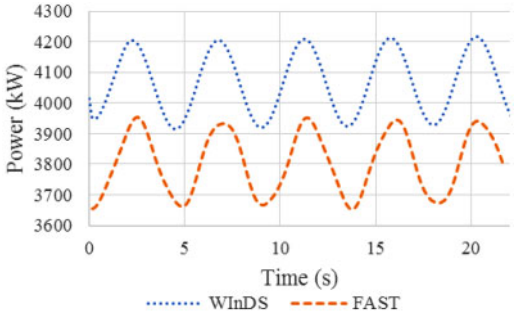

Figure 4. Time series of output power of rotor mounted on the spar for Case 6 with U = 10 m/s, H_m = 1.1 m, T_m = 4.5 s.

non-floating turbine. This comparison was expressed as a percentage calculated using the equation:

$$\varepsilon_{C\_P} = \{(C_{P,mean}/C_{P,fixed}) - 1\} \times 100 \quad (5)$$

where P = power performance characteristic; $C_{P,mean}$ = mean value of varying power coefficient from floating turbine; $C_{P,fixed}$ = steady value of power coefficient from non-floating turbine; and ε_{C_P} = percentage difference in performance between a floating and non-floating turbine. Therefore, positive results from this equation indicated better performance of the floating system over the non-floating system. These results were determined for each platform when experiencing each of the 6 motion cases for each wind speed listed in Table 2.

4 RESULTS

This section presents the results in the form of time series variations of output rotor power and bar charts comparing those obtained from *FAST* with those obtained from *WInDS*. In all bar charts the different motion cases are shown on the *x-axes*, where the number in brackets refers to the wind speed.

Figures 3 and 4 present the time series variations of output rotor power for the TLP and spar for case

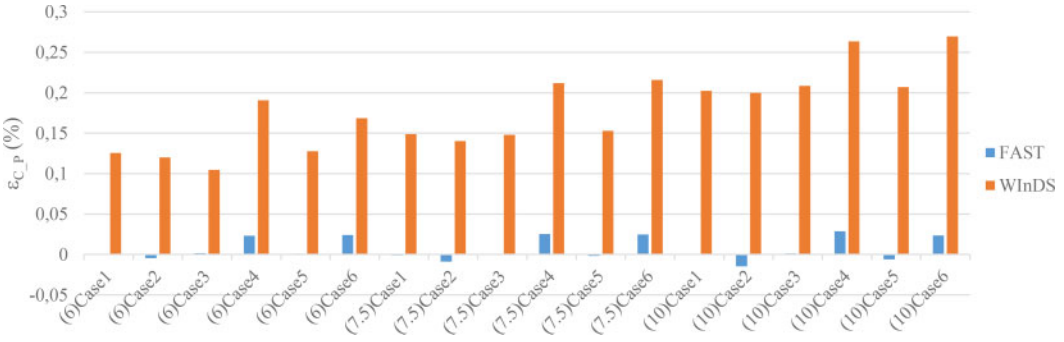

Figure 5. Comparison of *FAST* and *WInDS* results for power coefficient percentage differences between TLP and fixed non-floating system. On the x-axes the values in brackets refer to the wind speed.

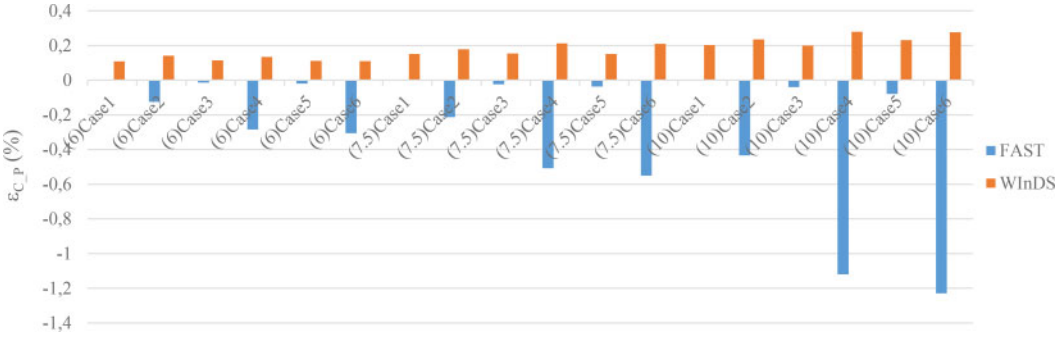

Figure 6. Comparison of *FAST* and *WInDS* results for power coefficient percentage differences between spar and fixed non-floating system.

6 motion at a wind speed of 10 m/s. There are two main observations to be made from these figures: the *WInDS* predictions are larger than those from *FAST*, and that the power fluctuation is substantial. These observations are discussed through the subsequent charts which compare the *FAST* and *WInDS* results.

With respect to the bar charts the results for percentage differences will first be discussed. From Figures 5 and 6, for the TLP and spar, respectively, it is clear that the largest values for ε_{C_P} noted by both *FAST* and *WInDS* occur in cases 2, 4, and 6 for both platforms. Since only these cases involve pitch motion this may be attributed to the increased unsteadiness that this motion induces. In all cases, heave is seen to contribute least to performance influences. As may be seen from Figure 6, the percentage differences for the spar from *FAST* are negative, implying a reduction in the time-averaged power coefficient compared to fixed conditions. Pitch motion causes the rotor plane to misalign itself with the wind, causing a reduction in efficiency. The TLP offers greater resistance to pitch motion than the spar, as evidenced by much greater magnitudes than those for the TLP.

From Figure 5, *WInDS* predicts greater percentage differences than *FAST*, though the values are still very small. These predictions are also very similar in magnitude to those in Figure 6. It was noted that these results were found to be of the same order as the convergence errors registered during the *WInDS* numerical convergence study. Therefore, whilst they seem to follow the same trends as those predicted by *FAST*, the actual values may be masked by numerical convergence errors in the free-wake computation. The small values make it very difficult to clearly distinguish between the numerical errors and the actual values resulting from phenomena caused by platform motion. Despite this, Farrugia (2014) showed that for a TSR of 7, the percentage difference in power due to platform motion was approximately 1% for a surge frequency of 0.2Hz, which is similar to that applied here. Thus, minimal motion influence is also shown.

The influence of wind speed is also noticeable for all motion cases by the increasing percentage difference magnitudes for both platforms. This is attributable to the larger wave heights occurring at higher wind speeds and hence larger platform motions.

Referring to Figures 7 and 8, it can be seen that, in the case of the TLP, the mean power coefficient predicted by *FAST* may be considered to be independent of platform motion and wind speed. On the other hand slight variations in this mean are noted for the spar in cases 4 and 6. This explains all the near-zero percentages registered by *FAST* in Figure 5 and the increasing percentage differences for cases 4 and 6 in Figure 6. In these figures, the difference between

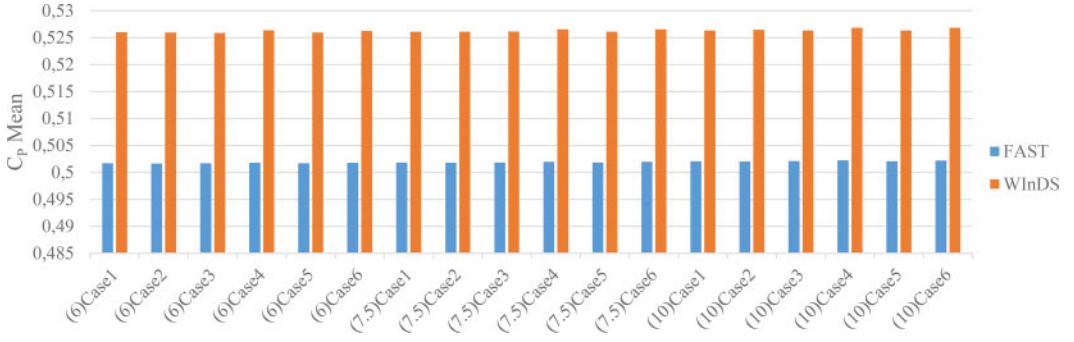

Figure 7. Comparison of *FAST* and *WInDS* results for mean values of varying power coefficient for the TLP.

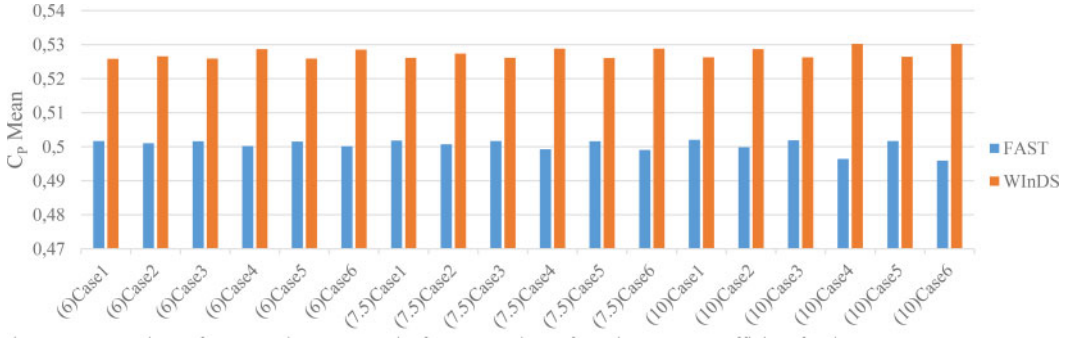

Figure 8. Comparison of *FAST* and *WInDS* results for mean values of varying power coefficient for the spar.

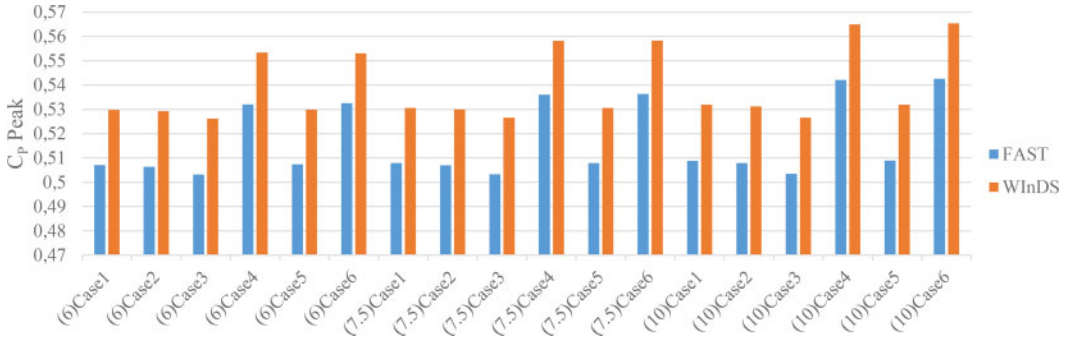

Figure 9. Comparison of *FAST* and *WInDS* results for peak values of varying power coefficient for the TLP.

the *FAST* and *WInDS* results is relatively constant. This difference follows from that registered during the derivation of the rotor performance curves for non-floating conditions (see Figure 1). Therefore, the difference here is attributed once again to the different ways in which *FAST* and *WInDS* model the influence of the wake-induced velocity at the rotor.

Overall, the percentage differences registered by both modelling tools show that the influence of platform motion on the time-averaged power coefficient is negligible. However, as was seen from Figures 3 and 4, the impact of platform motion on the time series of power performance variation is considerable. This may also be observed from the power coefficient peaks in Figures 9 and 10, and from the amplitudes of power variation in Figures 11 and 12. Here, the 'amplitude' refers to the difference between the peak and time-averaged values. In both sets of figures, the dominance of the pitch motion on performance variation is evident. The smallest impact results from heave motion. All peaks and amplitudes increase with wind speed due to the presence of larger waves.

The results from *FAST* and *WInDS* also seem to agree favourably in Figures 11 and 12, with the amplitudes from *WInDS* being slightly smaller than those from *FAST*. This discrepancy between the tools is more pronounced for cases involving pitch, especially for the spar. Despite the limitations in the BEM/GDW

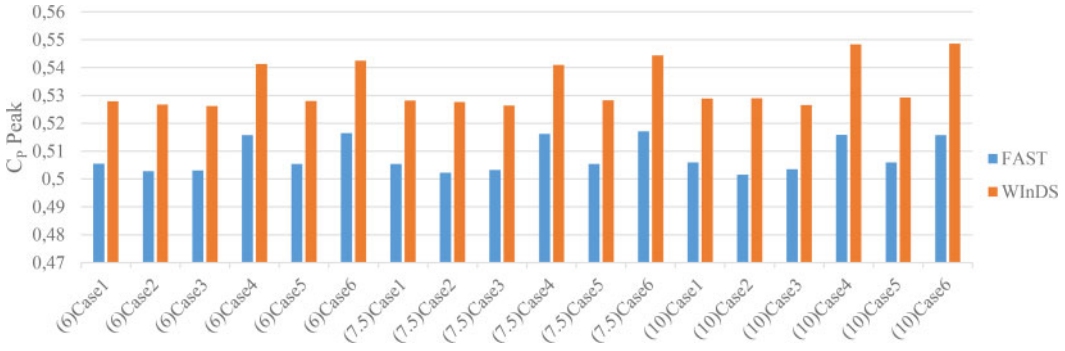

Figure 10. Comparison of *FAST* and *WInDS* results for peak values of varying power coefficient for the spar.

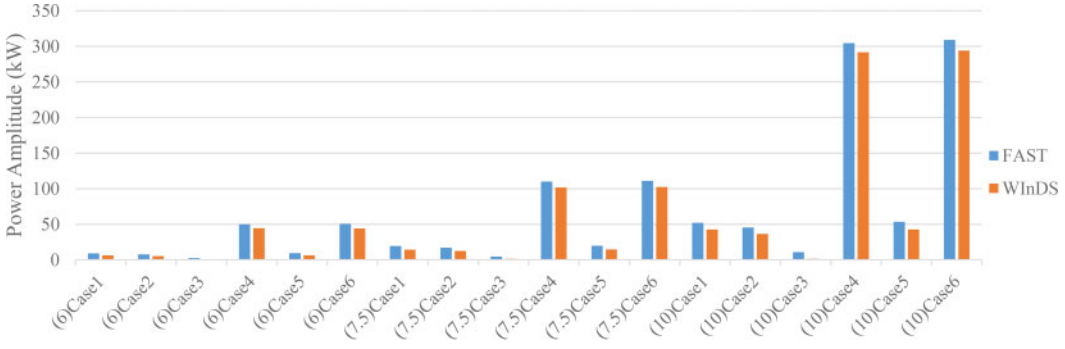

Figure 11. Comparison of *FAST* and *WInDS* results for amplitudes of varying rotor power output for the TLP.

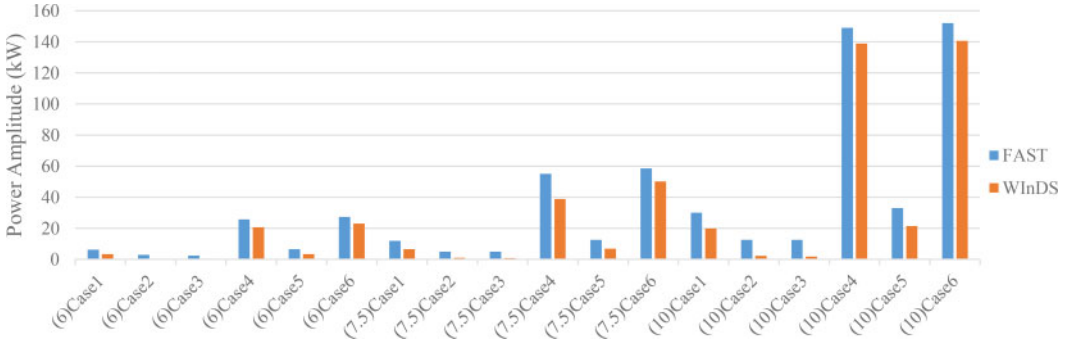

Figure 12. Comparison of *FAST* and *WInDS* results for amplitudes of varying rotor power output for the spar.

aerodynamic models as compared to free-wake vortex models, comparable predictions for the power amplitudes of variation could still be produced by *FAST* at a fraction of the computational cost of that incurred by *WInDS*.

While the negligible changes in mean power coefficient are being predicted, the estimates for the fluctuating component of the power coefficient are significant. In fact, the maximum peak-to-peak power from *WInDS* for case 6 at 10 m/s was estimated to reach 7.3 and 3.5% of the time-average value for the TLP and spar, respectively. It is also clear that a wind turbine on a TLP experiences larger peak-to-peak variations than one operating on a spar. From Figure 11, the TLP experiences a peak-to-peak power variation of approximately 600 kW for case 6 motion at a wind speed of 10 m/s. This puts higher demands on the control system, since with such a variation at this wind speed, the rotor power would continuously and periodically fluctuate about the rated power value.

5 CONCLUSIONS

This project sought to investigate the influences of floating platform dynamics on the power performance output of OFWTs under simple flow conditions involving a constant wind speed and regular waves.

By simulating various combinations of DOFs, wind speeds, and wave conditions it was possible to analyse which particular combination of conditions had the most significant influence on the power output. The numerical investigation involved the use of the BEM/GDW method in *FAST* and FVM forming the basis of *WInDS*. The main conclusions from this study are summarised below:

- The *WInDS* power coefficient results from the NREL turbine on a rigid base were greater than those obtained from *FAST* results. The same deviation also followed under floating conditions. The deviation at the optimal TSR, which is in fact also the maximum operating value, was found to be small and results from the differences in the inherent physical assumptions of the numerical models embedded in the codes. The availability of power measurement data for model floating turbines tested under strictly controlled wind and wave conditions is a crucial step to determine which model is most reliable.
- Percentage differences of time-averaged output rotor power between floating and non-floating turbines were consistently estimated to be very small ($<1.4\%$) by both *FAST* and *WInDS*.
- Both turbines on TLP and spar platforms experienced greatest performance variations when subjected to coupled surge, pitch, and heave motions, with dominant DOFs for the TLP and spar being surge and pitch, respectively.
- The time-averaged values for the rotor power for the turbine on a TLP were predicted to be independent of wind speed and motion DOFs. In the case of the turbine modelled on a floating spar, these values decreased with increasing wind speed under conditions involving coupled surge and pitch motion.
- Despite the negligible changes in overall mean performance, platform motion induces substantial fluctuation in the rotor output power. This has implications on the quality of power from floating wind turbines operating below the rated wind speed. The peak-to-peak variations in the rotor power from the turbine modelled on a TLP were found to be significantly higher than that operating on the spar.
- Despite limitations in the theories, *FAST* results were still in close agreement with those estimated by *WInDS*.

ACKNOWLEDGEMENTS

The research disclosed in this publication is partially funded by the MASTER it! Scholarship Scheme (Malta). The scholarship is part-financed by the European Union – European Social Fund.

REFERENCES

Aquilina, M., Sant, T., and Farrugia, R.N., 2014. Cost modelling of floating wind farms with upscaled rotors in Maltese waters. In: Sustainable Energy 2014: *The ISE Annual Conference*. Qawra, Malta, 20 March 2014. University of Malta.

BMT ARGOSS, 2014. *Wave Climate*. [online] Available at: <http://www.waveclimate.com> [Accessed 14 May 2014].

Butterfield, S., Musial, W., Jonkman, J.M., and Sclavounos, P., 2005. Engineering challenges for floating offshore wind turbines. In: *Copenhagen Offshore Wind Conference*. Copen-hagen, Denmark, 26–28 October 2005. Golden, CO: NREL.

European Wind Energy Association, 2013. *Deep Water – The Next Step for Offshore Wind Energy*. Brussels: EWEA.

Farrugia, R., Sant, T., and Micallef, D., 2014. Investigating the aerodynamic performance of a model offshore floating wind turbine. *Renewable Energy*, 70, pp. 24–30.

Henderson, A.R. and Patel, M.H., 2003. On the Modelling of a Floating Offshore Wind Turbine. *Wind Energy*, 6(1), pp. 53–86.

Hewson, E.W., 1975. Generation of power from the wind. *Bulletin of the American Meteorological Society*, 56(7), pp. 660–675.

Jonkman, J.M., 2007. *Dynamics Modelling and Loads Analysis of an Offshore Floating Wind Turbine*. NREL/TP-500-41958. Golden, CO (USA): NREL.

Jonkman, J.M., 2010. *Definition of the Floating System for Phase IV of OC3*. NREL/TP-500-47535. Golden, CO: NREL.

Jonkman, J.M. and Buhl, Jr, M. L., 2005. *FAST User's Guide*. Golden, CO (USA): NREL.

Jonkman, J.M., Butterfield, S., Musial, W. and Scott, G., 2009. *Definition of a 5-MW Reference Wind Turbine for Offshore System Development*. NREL/TP-500-38060. Golden, CO:NREL.

Leishman, J.G., 2006. *Principles of Helicopter Aerodynamics*. Cambridge University Press.

Matha, D., 2009. *Model Development and Loads Analysis of an Offshore Wind Turbine on a Tension Leg Platform, with a Comparison to Other Floating Turbine Concepts*. NREL/SR-500-45891. Golden, CO: NREL.

Moriarty, P.J., and Hansen, A.C., 2005. *AeroDyn Theory Manual*. Golden, CO, USA: NREL.

Sant T., 2007. *Improving BEM-based aerodynamic models in wind turbine design codes*. Ph.D. Delft University of Technology. Available: http://www.tudelft.nl.

Sebastian, T., 2012. *The Aerodynamics and Near Wake of an Offshore Floating Horizontal Axis Wind Turbine.* Ph.D. University of Massachusetts Amherst.

Withee, J.E., 2004. *Fully Coupled Dynamic Analysis of Floating Wind Turbine System*. Ph.D. Massachusetts Institute of Technology.